Since January 2020 Elsevier has created a COVID-19 resource centre with free information in English and Mandarin on the novel coronavirus COVID-19. The COVID-19 resource centre is hosted on Elsevier Connect, the company's public news and information website.

Analytica Chimica Acta 1226 (2022) 340286

Contents lists available at ScienceDirect

Analytica Chimica Acta

journal homepage: www.elsevier.com/locate/aca

Visual diagnosis of COVID-19 disease based on serum metabolites using a paper-based electronic tongue

Mohammad Mahdi Bordbar [a], Hosein Samadinia [a], Azarmidokht Sheini [b], Jasem Aboonajmi [c], Pegah Hashemi [d], Hosein Khoshsafar [a], Raheleh Halabian [e], Akbar Khanmohammadi [d], B. Fatemeh Nobakht M. Gh [a], Hashem Sharghi [c], Mostafa Ghanei [a], Hasan Bagheri [a,*]

[a] Chemical Injuries Research Center, Systems Biology and Poisonings Institute, Baqiyatallah University of Medical Sciences, Tehran, Iran
[b] Department of Mechanical Engineering, Shohadaye Hoveizeh Campus of Technology, Shahid Chamran University of Ahvaz, Dashte Azadegan, Khuzestan, Iran
[c] Department of Chemistry, College of Sciences, Shiraz University, Shiraz, Iran
[d] Research and Development Department, Farin Behbood Tashkhis LTD, Tehran, Iran
[e] Applied Microbiology Research Center, Systems Biology and Poising Institute, Baqiyatallah University of Medical Sciences, Tehran, Iran

HIGHLIGHTS

- An optoelectronic tongue was fabricated by non-specific receptors for detection of serum metabolites.
- The sensor was used to discriminate patients infected by COVID-19 from healthy controls.
- The discrimination analysis was achieved by comparison between the total responses of patient and healthy classes.
- The severity of the disease and the viral load associated with PCR analysis were estimated.

GRAPHICAL ABSTRACT

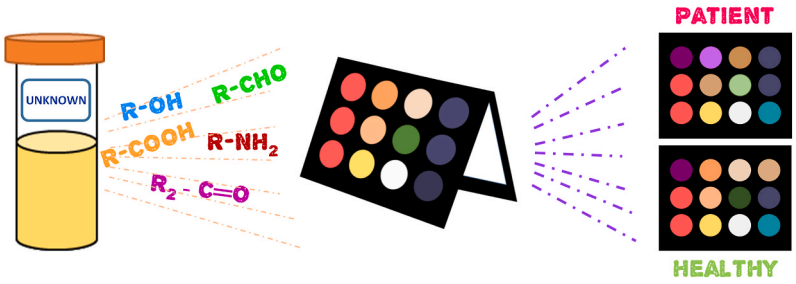

ARTICLE INFO

Keywords:
Array-based sensor
Colorimetric detection
COVID-19
Metabolomics
Rapid detection
Chemometrics

ABSTRACT

This study aims to use a paper-based sensor array for point-of-care detection of COVID-19 diseases. Various chemical compounds such as nanoparticles, organic dyes and metal ion complexes were employed as sensing elements in the array fabrication, capturing the metabolites of human serum samples. The viral infection caused the type and concentration of serum compositions to change, resulting in different color responses for the infected and control samples. For this purpose, 118 serum samples of COVID-19 patients and non-COVID controls both men and women with the age range of 14–88 years were collected. The serum samples were initially subjected to the sensor, followed by monitoring the variation in the color of sensing elements for 5 min using a scanner. By taking into consideration the statistical information, this method was capable of discriminating COVID-19 patients and control samples with 83.0% accuracy. The variation of age did not influence the colorimetric patterns. The desirable correlation was observed between the sensor responses and viral load values calculated by the PCR test, proposing a rapid and facile way to estimate the disease severity. Compared to other rapid detection methods, the developed assay is cost-effective and user-friendly, allowing for screening COVID-19 diseases reliably.

* Corresponding author. ;
E-mail addresses: h.bagheri@bmsu.ac.ir, h.bagheri82@gmail.com (H. Bagheri).

https://doi.org/10.1016/j.aca.2022.340286
Received 7 April 2022; Received in revised form 5 August 2022; Accepted 17 August 2022
Available online 22 August 2022

1. Introduction

As a new kind of respiratory infectious disease, COVID-19 virus has infected and killed many people since 2019 [1]. The virus is highly contagious, contaminating and disordering the lung function [2]. The World Health Organization (WHO) has introduced effective ways such as chest imaging and polymerase chain reaction (PCR) for the diagnosis and control of the disease [3]. Although these methods provide reliable information about the disease severity, they face serious limitations such as the need of a specialized operator for imaging and sampling, expensive devices, and a long delivery time of the results. Also, the patient should attend the medical clinics. It is possible that a false negative result is indicated by the PCR test due to the inappropriate sampling process, contamination of the sample, errors in the extraction of biological materials and PCR inhibiting factors [4].

The sensing methods based on nucleic acid amplification or antigen detection have been developed to detect COVID-19 [5,6]. These sensors use optical and electrochemical transducers that digitize changes in the properties of the sensing element bonded to a bioreceptor [7]. Compared to PCR, the sensing methods have a shorter detection time, and show higher sensitivity for the diagnosis of patients [8]. However, they suffer from the costly and time-consuming fabrication process, and require special storage conditions [9].

The viral infection disrupts the body's immune system, leading to changes in the body's metabolites [10]. The chemical structure of metabolites comprises aromatic or aliphatic hydrocarbons with acidic, amino, aldehyde, ketone, and hydroxyl substitutions [11]. Since these compounds are released into the bloodstream, metabolic changes caused by a disorder can be monitored by analyzing this biofluid [12]. The evaluation of the serum chemical profiles provides better information in comparison to plasma. This is because the volume of the matrix containing the small molecules decreases after the removal of coagulation proteins, resulting in pre-concentration, and subsequently, more accurate identification of metabolites [13].

The instrumental methods such as LC-MS, GC-MS and NMR spectroscopy provide useful information about differences in the serum metabolites of healthy people and patients with COVID-19 [14–17]. Based on the published reports, the concentration of compounds such as R–S lactoglutathione and glutamine, and other essential amino acids in the patient decreases, whereas the amount of chemical species, including hypoxanthine, inosine, acetone, acetoacetic acid, 3-hydroxybutyric acid, glucose, succinate and pyruvate, 2-hydroxybutyric acid, lactic acid, ribonic acid, malic acid, pantothenic acid, and oxalic acid increasingly correlate with disease severity [14–17]. The validity of these traditional techniques is based on the unique responses for each sample, thereby screening and discriminating patient and healthy samples with high accuracy, and detecting significant markers related to the disease along with their concentrations. However, the analysis process requires specific laboratory conditions, and an operator to collect, prepare and perform the experiment, and funds for purchasing the complex devices, solvents, and reagents [18].

A short analysis time and possibility of on-site measurement are two important parameters for the rapid diagnosis and evaluation of the treatment process of COVID-19 disease [19]. Unlike the previous assays, the optical sensing devices are portable tools, being capable of quantifying the metabolites in a biological sample at an appropriate time [20]. As well, they are favorable due to their advantages such as their simple and cost-effective design, easy sampling process, and naked-eye responses. Depending on the number of sensing elements in the sensor structure, a specific species or a set of diverse chemical compounds can be identified with high selectivity [21].

The evaluation of metabolites of biological samples can be carried out using an array of sensing elements, providing high performance in the detection of volatile and thermally stable chemical species in the vapor phase (E-nose) [22], or low volatility materials in the liquid phase (E-tongue) [23]. Compared to E-noses, the sample detection using E-tongue-based sensors is conducted without requiring thermal instruments (e.g., an oven or a heater) and carrier gas flow (N_2). To fabricate these sensors, the paper substrates has recently gained more attention since they facilitate the fabrication of sensors with different designs, and the immobilization of sensing elements on the paper surface. Moreover, the analyte can flow on the paper substrate surface without applying any external force [24].

Owing to the paper flexibility, these sensors can be fabricated in a 3D configuration such as origami structure, thus reducing the analysis time and consuming a low volume of the sample. Also, the color of biological samples does not influence the color changes caused by the interaction of sensing elements with chemical markers [25]. The performance of arrays depends on the components of the detection zone, being composed of selective cross-reactive sensing elements [26]. The optical properties of these sensors are different before and after the interaction with the analytes. Since changes can happen due to the release of hydronium ions, replacement of analyte with a ligand in the complex structure, nucleophilic and hydrophobic interactions, electrostatic connection, and hydrogen bonding to an electronegative atom, it is possible to employ pH-sensitive indicators, metal ion complexes, metalloporphyrins and nanoparticles as the sensing elements [27]. The use of receptors with diverse intrinsic properties increases the sensor's ability to recognize the compounds with different structures and concentration ranges. This feature helps the sensor track minor changes of the type and concentration of chemical species in a biological sample, thereby diagnosing a disease.

Designing colorimetric sensors to diagnose diseases through metabolites released in biological samples has been one of the goals of our research team in recent years. In the case of COVID 19, we proposed various sensors to detect this disease by analysis of the metabolites of saliva samples [28], exhaled breath [29] and urine samples [30]. In this paper, a new approach is proposed based on designing an optical sensor array with origami configuration, allowing for detection of the COVID-19 disease and discrimination between COVID-19 patients and non-COVID controls by the serum samples. To the best of our knowledge, nevertheless, paper-based electronic tongues have not been reported for the detection of viral infections by the monitoring of serum sample metabolites. Twelve sensing elements are included in the array structure, which may be discolored after interacting with the serum materials. This provides a unique pattern for each COVID-19 patients and non-COVID samples. The results obtained from the sensor are explored visually and by image software. They are also proved via multivariate statistical methods. On the other hand, the effects of some parameters such as the concentration and composition of receptors, age of participants, and disease severity on the sensor response are investigated.

2. Experimental section

2.1. Materials and solution

The sensor substrate was fabricated by Whatman® Grade NO.2 filter paper. The chemical solids such as iron(II) chloride tetrahydrate ($Fecl_2.4H_2O$), gold (III) chloride trihydrate ($HAuCl_4.3H_2O$), copper(II) nitrate trihydrate ($Cu(NO3)_2.3H_2O$), boric acid (H_3BO_3), sodium borohydride ($NaBH_4$), bromocresol purple (R1), sodium hydroxide (NaOH), and the solvents including ethanol (EtOH), sulfuric acid (H_2SO_4) were obtained from Merck chemical company. The organic dyes (pyrocatechol violet (Py), 2, 4-dinitrophenylhydrazine and bromophenol red (R2)), the reducing and stabilizing agents (sodium citrate, poly glutamic acid (PGA), Bovine serum albumin (BSA), caffeic acid (CA)) and the other materials (phenylboronic acid (PBA), vanadyl sulfate pentahydrate ($VOSO_4.5H_2O$)) were provided from Sigma Aldrich. Porphyrin structures were achieved from Sharghi's laboratory, Shiraz, Iran. The experimental procedures for providing these materials consisting of meso-tetrakis(4-hydroxyphenyl) porphyrin-manganese (III) acetate (Mn

(III)T(4-OH)PP(OAC)) meso-tetraphenylporphyrin]Iron(III) chloride (Fe(III)TPPCl) and [meso-tetraphenylporphyrin]-Tin (II) (Sn(II)TPP) were described in the previous studies [31–33].

The solution of organic dyes such as R1, R2 and porphyrin were made by dissolving a certain amount of these materials in a specified volume of EtOH. To prepare the solution of pyrocatechol violet and the metal ion salts, the deionized water was used. DWES was a yellow solution containing 0.4 g 2, 4-dinitrophenylhydrazine dissolved in the mixing solvent including 10.0 mL EtOH and 3.0 mL deionized water. The product was acidified by 2.0 mL H_2SO_4 and homogenized on the stirrer during 10 min. To remove the undissolved particles, the mixture was filtered and the clear solution was used for further studies [34].

2.2. Apparatus and software

In this study, the devices such as Metrohm 632 pH-meter (Model 780 pH lab), micropipette (BRAND Transferpette® S, Germany), HP LaserJet printer 1200 and canon scanner (CanoScan LiDE 220) were used to adjust the pH of media, immobilize the sensing element on the surface of filter paper, print the sensor structure on the paper and capture and save the photos of sensor, respectively. The sensor structure were designed in the AutoCAD 2016 environment. The image of sensor was evaluated by Image J (1.51n, National Institutes of Health, USA) software. The results of multivariate and bio statistical analysis were obtained by MATLAB R2015 and SPSS (Version 22; Chicago, IL, USA) software, respectively.

2.3. Sensing element preparation

The opto electronic tongue was created by accumulation of four different chemical structures as sensing elements such as gold nanoparticles (AuNPs), triaryl methane dyes, metalloporphyrins and metal ion complexes. To prepare the AuNPs, three individual capping or reducing agents including BSA, CA and PGA were used. BSA-AuNPs were prepared by addition of 3.0 mL BSA solution with the concentration of 20.0 mg/mL to 100.0 mL of citrate reduced AuNPs solution. The reaction was proceeded on the stirrer and complete after 20 h. The pure BSA-AuNPs was provided by removing the extra BSA particles during centrifuging (10000 rpm, 15 min) and re-dispersing the residue in the deionized water [35]. To have CA-AuNPs, 60.0 μL of $HAuCl_4$ (1.0×10^{-2} mol/L) and 280.0 μL of CA (5.0×10^{-3} mol/L) were combined together and injected to a flask containing 3660.0 μL of deionized water. The flask was homogeneously stirred for 4 h. During this time, the experiment was performed under reflux condition and the reaction temperature was adjusted at 50 °C. The red resulting solution was used for further studies [36]. PGA-AuNPs were fabricated by mixing 5.0×10^{-2} mol/L of $HAucl_4$ (20.0 mL), 3.0×10^{-2} mol/L D-glucose (10.0 mL) and 0.1% W/V PGA (1.0 mL) followed by dropwise addition of 0.5 mol/L NaOH solution (280.0 μL) [37,38]. The solutions of prepared NPs were converted to dried particles using a laboratory freeze-dryer. The products was homogenized in a mortar and kept in the sterile tubes before usage. To provide the NPs based sensing elements, the aqueous solution of each NPs powder was prepared at the optimum concentration.

The second set of sensing elements were produced by addition of the optimum volume of DWES or PBA (2.0 mol/L) solutions to triarylmethan dyes solutions (R1 and R2) with the specified volume and concentration. However, the optimal amount of porphyrins powders were dissolved in the 1.0 mL of EtOH to form the third class of sensing elements. The last colorimetric receptors in the array structure are the complexes obtained by binding the Py (50.0 μL) to metal ions such as V (IV), Fe (II) and Cu (II) ions (50 μL). The reaction was performed in a borate buffer (100.0 μL, 0.1 mol/L and pH = 9.0) [39]. The concentrations of ligand and metal ion should be optimized.

Table 1
Demographic data of the studied samples.

Variable	Non-COVID controls	Patient with COVID-19
Number	56	62
Sex		
Male	32	32
Female	24	30
Age (Mean ± SD)	51.14 (±16.94)	56.98 (±14.67)
RT-PCR*	Negative	Positive
N gene**		23.98 (13–34)
RdRp gene**		24.08 (14–35)
Total response***	219.63 (±41.62)	240.34 (±37.10)

* RT-PCR: Reverse transcription polymerase chain reaction.
** Data are represented as median and interquartile range.
*** P-value < 0.005.

2.4. Sample collection

This study was carried out on the residuals of serum samples of COVID-19 patients and non-COVID patients with coded and unattributable information who admitted to Baqiyatallah Hospital from 2020 to 2021. The serum samples obtained from clinical laboratory of hospital before their final disposal. The total number of samples was 118 (62 patient and 56 control samples). The patient samples were selected who did not take any medication before the appointment, and the results of their chest imaging and rRT-PCR test had been confirmed by a pulmonologist. The control samples were selected from non-COVID patients [28–30]. The demographic information is summarized in Table 1.

2.5. Fabrication of opto-electronic tongue

The structure of the proposed sensor is shown schematically in Fig. 1a. The pattern was drawn by the design software (AutoCAD). The sensor is in the form of a rectangle with dimensions of 1.5 cm × 1 cm, being divided into two parts: the injection zone (the white rectangle) for subjecting the serum sample, and the detection zone (12 small circles) for immobilizing the sensing elements. To make the black areas hydrophobic, the paper was heated at 200 °C for 45 min after printing the proposed pattern on its surface [40]. By injecting 0.12 μL of sensing elements on the circles of the detection zone, the desired sensor array was fabricated (see Fig. 1).

2.6. Detection method

Scheme 1 summarized the all experimental procedures for this study. As seen, the sensor was fabricated on filter paper with high flexibility that could be folded from the middle of substrate. The sensor was sealed between two holders, so that the injection zone completely covered all the circles of the detection zone. The top layer of the holder had a hole that helped add the serum sample (20.0 μL) of each participant to the injection zone. Due to the capillary nature of the paper, the sample spread well on the surface of the substrate. The interaction between the serum sample and the sensing elements was allowed to be complete for 5 min. A scanner was used to collect images of the sensor after its fabrication, and also after exposing it to the serum sample. The information of each image, containing the mean values of red, green and blue color components of each sensing element, was extracted with ImageJ software. The difference in the RGB values of each sensing element was calculated from the following relations:

$$\Delta R = R_{Final} - R_{Initial}$$

$$\Delta G = G_{Final} - G_{Initial}$$

$$\Delta B = B_{Final} - B_{Initial}$$

The data obtained from the image processing was collected in a data

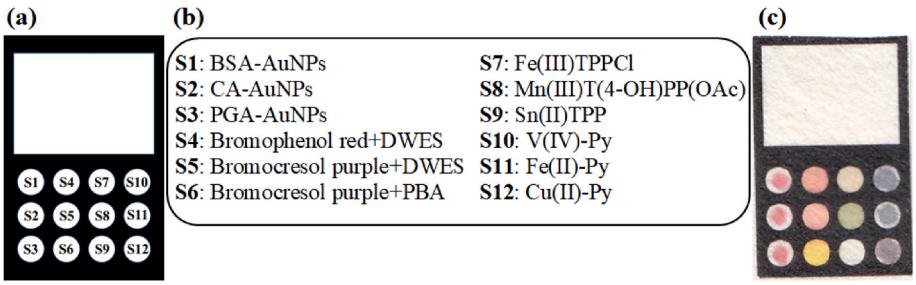

Fig. 1. (a) The proposed pattern of the sensor, (b) the list of sensing elements and (c) the fabricated paper based E-tongue.

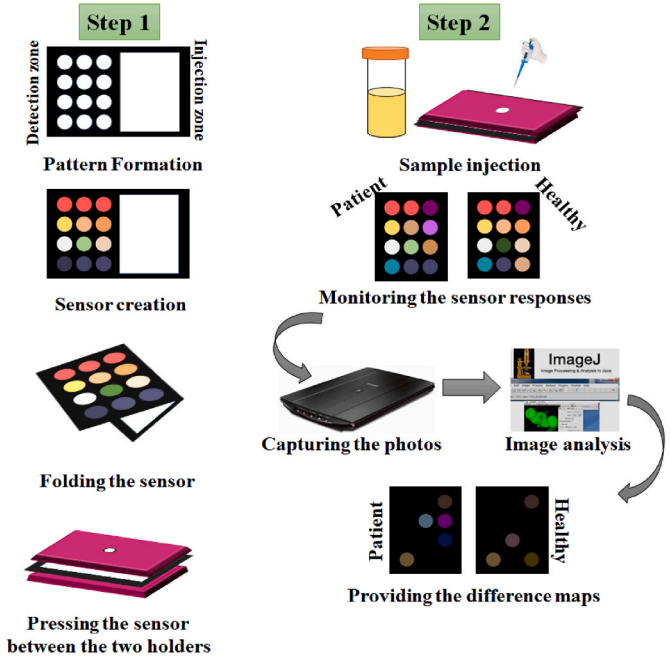

Scheme 1. The schematic diagram for designing, fabricating and ability of the proposed paper based E-tongue.

vector comprised of 36 members (12 sensing elements × 3 color components).

2.7. Data processing

Statistical analysis was performed in two (qualitative and quantitative) sections. The qualitative section described the evaluation of the sensor ability to discriminate between the two (healthy and patient) studied groups. The quantitative section explained the procedure for calculation of the sensor responses to all the studied serum samples, as well as the correlation between the sensor responses and different parameters. Concerning the qualitative section, the data vectors made for the analysis of 118 serum samples were placed in a data matrix with a size of 118 × 36, and the distinction patterns were explored using the principle component analysis-discriminate analysis (PCA-DA) method.

For the quantitative section, the total sensor response was obtained by calculating the Euclidean norm of the data vector based on the following equation:

$$Euclidean\ Norm = \sqrt{\sum_{i=1}^{n} (x_i^2)}$$

where x_i is the ith component of the data vector for each serum sample. To acquire the total response of each sensing element, the Euclidean norm of its color component values was computed.

The two independent sample *t*-test, and Pearson correlation coefficient were used to compare between mean total sensor responses of the COVID-19 patients and non-COVID control groups, and to find an effective relationship between changes in the total sensor response (or the total response of a sensing element) and the increase or decrease in the numerical amounts of some parameters such as age, disease severity and viral load value, respectively.

2.8. Discrimination ability function

As a mathematical function, the discrimination ability function (DAF) was used to find the optimal value of effective parameters in this experiment [41]. In fact, it is possible to achieve the best discrimination between patients and control individuals through DAF. The following equation is defined to calculate DAF:

$$DAF = \frac{N\sum_i (\overline{Y}_i - \overline{\overline{Y}})^2}{\sum_i \sum_j \left(Y_{ij} - \overline{Y}_i\right)^2}$$

where N is the number of groups (patients and control individuals) participating in this study. Y_{ij} is the Euclidean norm for the jth sample in the ith group, $\overline{Y}_i$ is the mean of all Euclidean norms obtained for samples of the ith group, and $\overline{\overline{Y}}$ is the average of Euclidean norms calculated for all the samples studied in this experiment. Note that, the optimal value of each parameter has the highest DAF value.

3. Results and discussion

Basically, COVID-19 infection decreases the concentration of amino acids, and increases the accumulation of carboxylic acids, aldehydes, sugars, alpha-keto acids and heterocyclic amines in the serum sample [14–17and28-30]. Monitoring these changes with a reliable sensor can help rapidly detect and treat the disease. The recognition of minor differences between the metabolic profiles of patient and control samples can be performed by an electronic tongue including a set of sensing elements with different chemical structures [28–30]. Here, the efficiency of the electronic tongue is investigated to detect and differentiate between the metabolites of serum samples collected from the COVID-19 patients and non-COVID individuals. The device contains AuNPs modified by BSA, CA and PGA, two organic dyes that mixed by DWES and PBA, metalloporphyrins with the metal core of Fe, Mn and Sn and metal ion complex fabricating by mixing Py with three ions of V (IV), Fe (II) and Cu (II), individually.

The interaction of metabolites and NPs based sensing elements depends on the metal core and coating agent properties causing NPs have different electrical charge or covered by different functional groups [42]. Due to this conditions, NPs can participate in different electrostatic, H-bonding, covalent or nucleophilic interactions [42]. Of course, they are synthesized in the different size, therefore, the larger nanoparticles may not be able to bind with the massive metabolites because of steric hindrance while smaller particles interact easily with the same

(a)

Number of experiment	Description
EX 1	NPs (1.0 mg.mL^{-1}), Organic dyes* (1.5 mg.mL^{-1}), Porphyrins (3.0 mg.mL^{-1}), Metal complexes** (0.01 M)
EX 2	NPs (1.5 mg.mL^{-1}), Organic dyes* (2.0 mg.mL^{-1}), Porphyrins (4.5 mg.mL^{-1}), Metal complexes** (0.05 M)
EX 3	NPs (2.0 mg.mL^{-1}), Organic dyes* (2.5 mg.mL^{-1}), Porphyrins (6.0 mg.mL^{-1}), Metal complexes** (0.10 M)
EX 4	NPs (2.5 mg.mL^{-1}), Organic dyes* (3.0 mg.mL^{-1}), Porphyrins (7.5 mg.mL^{-1}), Metal complexes** (0.15 M)

* Organic dyes were combined with DWES and PBA with ratio of 1:1 V/V
** Metal complexes were mixed in the borate buffer (0.1 M).

(b)

Number of experiment	The volume ratio of (reagent*: additive**)
EX 1	1:1
EX 2	2:1
EX 3	3:1
EX 4	4:1
EX 5	5:1

*Reagents are organic dyes.
** Additives are DWES and PBA.

(c)

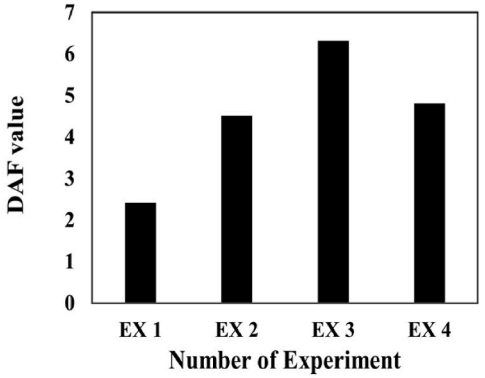

(d)

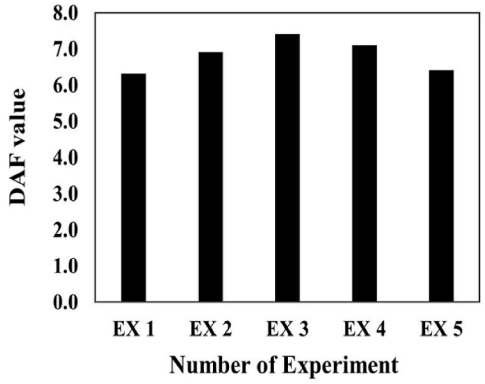

(e)

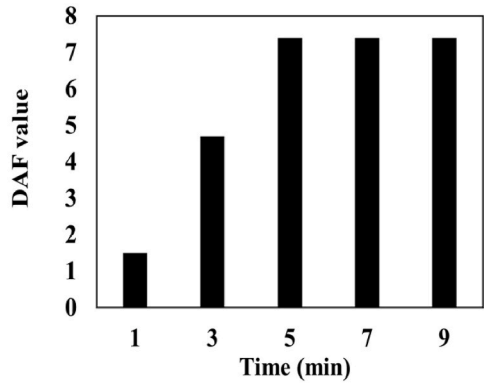

Fig. 2. The optimal conditions: (a) The guideline and (b) the respective DAF plot for providing sensing elements with a specified concentration, (c) The guideline and (d) the respective DAF plot for the preparation of organic dyes-additives mixture, (e) the DAF plot for finding the response time for the proposed sensor.

materials [42]. In second set of sensing elements, the dyes R1 and R2 are combined by two additives of DWES and PBA. The additives can trap aldehyde and diol compounds, respectively [34,43], thus changing the proton concentration in the environment. These variations can be detected by organic dyes which are sensitive to hydronium ions. This event cause the color of dyes turns proportional to pH changes. Metalloporphyrins are comprised of a heterocyclic macromolecule with a central nucleus of various metal ions. They tends to have an acid-base interaction with particular chemical species. The chemical hardness and affinity of central nucleus and chemical species are important factor for this interaction [44]. The complexes consisting of a triarylmethane dye and metal ions are the final set of the proposed electronic tongue. These materials are capable to detect the compounds with acidic and amino groups [39,45]. Metal ions have a high affinity to a certain analyte and form a new complex of metal ion-analyte. It leads to release the organic dye from the complex structure, thereby changing the color of the sensing element. In the next hypothesis, the analyte may interact simultaneously with the metal ions and functional groups of the dye, forming a ternary configuration [28,29]. Each sensing elements are selective cross-reactive materials that respond to all metabolites in a typical biological sample with different intensity. Finally, a color pattern is obtained for each sample which is unique and shows the variation in

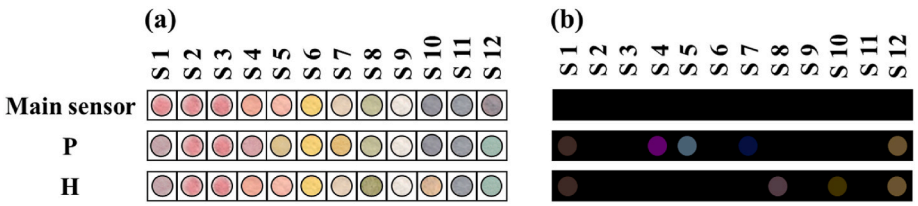

Fig. 3. (a) The responses of sensor and (b) the difference maps for patient infected by COVID-19 (P) and non-COVID control (H). The experiment performed in the optimum conditions described in Fig. 2.

the metabolic profile of a specified sample [28,29].

The full information about the performance of proposed electronic tongue, characterization of sensing elements, optimization, colorimetric observations, quantitative measurements and statistical analysis are described in the following subsections.

3.1. Characterization of synthesized NPs

To evaluate the synthesis process of AuNPs, the final product was used to calculate the UV–Vis spectrum, surface electrical charge and hydrodynamic size distribution. As shown in Fig. S1a, the absorption peak of NPs has a maximum intensity at 530 nm for BSA-AuNPs, 558 nm for CA-AuNPs and 520 nm for PGA-ANPs which is approximately similar to previous reports. Also, Fig. S1b shows that the negative electrical charge were distributed on the surface of all synthesized NPs, numerically were equal to −16, −35 and −34 mV for AuNPs prepared by BSA, CA and PGA, respectively. The NPs were synthesized with the average size of 30 nm (BSA-AuNPs), 25 nm (CA-AuNPs) and 25 nm (PGA-AuNPs) as presented in Fig. S1c.

3.2. Optimization

To obtain an acceptable difference between the metabolites of the patient and control serum samples, the sensor needs to be fabricated based on the optimal concentration of sensing elements. Also, the interaction of metabolite and the fabricated sensing elements should be complete during a specified time. In this regard, five serum samples were selected from both control and patient groups in order to optimize the values of the effective parameters. 20.0 μL of each sample was added to the sensor, and the experiment was repeated three times. For each sample, the total sensor response was calculated based on the Euclidean norm. The DAF equation was used to find the optimal value.

In the first step, each reagent was prepared in four different concentrations, as given in Fig. 2a. According to Fig. 2b, the distinction between infected and control samples is improved by increasing the reagent concentration. The highest DAF response is observed by the sensor fabricated based on the EX 3 pattern. However, the discriminatory performance of the sensor decreases at higher concentrations. At the optimized value, the reagents contain sufficient active sites for capturing the analyte, so that the initial color intensity of the receptors does not prevent the observation of the color changes induced by the interaction [46,47].

In the second step, DWES and PBA compounds were individually mixed by pH indicators in the array structure. The components of the resultant mixture were combined with five different volume ratios of (1: 1), (1: 2), (1: 3), (1: 4), and (1: 5) (see Fig. 2c). It is found that the use of a mixture of additives: pH indicator with the volume ratio of (1: 3) can lead to a larger difference between the patient and control samples (Fig. 2d). At other volume ratios, the change in the color of the pH indicator is reduced. The two reasons for this observation are the blockage of the functional groups of the indicators in the presence of additives with higher concentrations, and the detection of the lower amounts of metabolites containing aldehyde and diol groups due to the lower additive concentrations in the environment.

To find the time needed for the complete interaction between serum metabolites and sensing elements, the response of the sensor was evaluated within 1–9 min. Fig. 2e shows that the color changes of the sensing elements increase up to 5 min, beyond which no significant changes are observed in the sensor responses. This time was used as the optimal time to receive the sensor's information in the subsequent studies.

3.3. Sensor observations

The fabricated array was exposed to COVID-19 patient and non-COVID serum samples, and the colorimetric responses obtained are presented in Fig. 3a. As inferred, the results of sensing detection can be divided into four categories. (1) Sensing elements do not tend to interact with the serum metabolites of patients and control individuals. CA-AuNPs, PGA-AuNPs, PBA + bromocresol purple, Sn (II) TPP and Fe (II)- Py receptors do not discolor after injecting the analyte. (2) Sensor components such as BSA-AuNPs and Cu (II)- Py change color in the presence of chemical species in the matrix of both healthy and infected samples. (3) Chemical receptors such as DWES + bromophenol red, DWES + bromocresol purple, and Fe (III) TPPCl react only with infected specimens. (4) The response of sensing elements such as V (IV)-Py and Mn (III) T (4-OH) PP (OAC) is observed after being exposed to metabolites of the healthy sample.

The color difference maps were created by processing the resulting images of each sample using the image analysis software, providing more detailed information about the interaction between the sensor elements and analytes. The mono-color spots obtained by the difference between the mean values of each receptor's color component before and after the interaction with the analyte are depicted in Fig. 3b, giving rise to discrimination patterns with better clarity for the healthy and infected samples. Also, the color changes of the sensing elements S8, S10 and S12 are significantly noticeable. In total, 118 serum samples were studied using a diagnostic kit, and the respective colorimetric responses and color difference maps are given in Fig. S2 and Fig. S3. The bar graphs associated with the total responses (Euclidean norms) of the receptors after the exposure to the serum sample are depicted in Fig. S4. Although the sensors S1 and S12 respond to the chemical compositions of both patients and control serum samples, BSA-AuNPs (S1) shows a higher tendency to interact with infected serum metabolites. Moreover, Cu (II) -Py (S12) has stronger binding with the chemical species of the healthy serum samples. The comparison between responses of S8 and S10 indicates that the compounds of the healthy sample tend to react more with the porphyrin receptors than with metal ion complexes. This is because the enthalpy of Lewis acid-base interactions is higher than that of the indicator displacement assays [48]. Among the sensors sensitive to the infected samples, the responses of S4 and S5 are more intense than those of S7. Probably, the concentrations of aldehyde-functionalized species are higher in the infected samples, which can be detected by a specific receptor such as DWES. Moreover, bromophenol red outperformed bromocresol purple in tracking the changes in the pH of media.

During the implementation of the study, the most of the patients who visited the hospital were infected with COVID-19, and people with other respiratory viral diseases were approximately unavailable. However, to evaluate the reliability of the method, the proposed sensor was exposed to other viruses that are detectable through metabolites of serum sample

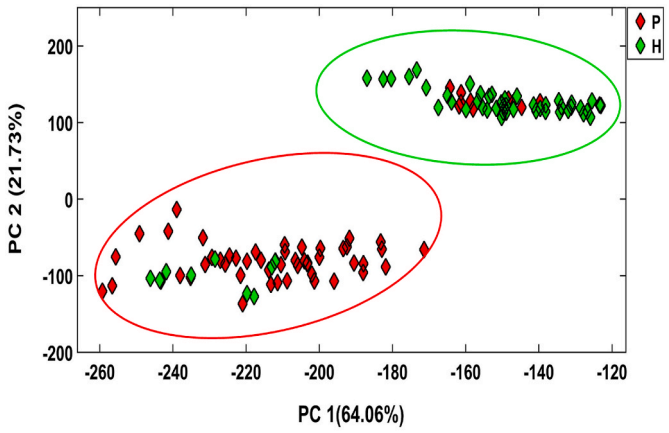

Fig. 4. PCA score plot for discrimination of 118 patient and control samples. The experiment performed in the optimum conditions described in Fig. 2.

Table 2
Statistical parameters for PCA-DA analysis.

Error rate: 17.0% Accuracy: 83.0%		
Sample	Sensitivity (%)	Specificity (%)
Patien	82.2	83.9
Control	83.9	82.2

such as cytomegalovirus (CMV) and BK virus (BKV) (see Fig. S5). As illustrated, the sensing element of S4 responded to serum metabolites of patients caused by all studied virus. On the other hands, the color of S5 and S7 changed in the presence of serum components infecting by only COVID-19, S3 interacted with metabolites of BKV and S9 shows the variation in the metabolic profile of a person with CMV. Therefore, the other types of virus did not influence on the color pattern of the electronic tongue related to patients caused by COVID-19, indicating the high selectivity of the proposed sensor.

3.4. Statistical pattern recognition

As a statistical multivariate method, PCA-DA was used to find the discrimination pattern between patient and control samples. The PCA-DA model was developed by a matrix made of 118 data vectors. The PCA score plot drawn by the first two principle components (PCs) is shown in Fig. 4, having an 85.8% distribution of the total explained variance. While more than two PCs are needed to extract 95% of the important information of the data matrix, this plot indicates that a good distinction can be made between the two studied groups using the first two PCs. As observed, the proposed sensor classifies 51 patients and 47 control samples in their native groups. However, 20 of the total samples are not correctly detected. The sensitivity of the sensor for detection of healthy individuals and those infected by COVID-19 is found to be 83.9% and 82.2%, respectively. In addition, the total accuracy for discriminating the patients from the control samples is calculated to be 83.0%. The parameters provided by the classification analysis are summarized in Table 2.

3.5. Total sensor response-based discrimination analysis

By calculating Euclidean norms of the data vector obtained for 62 infected and 56 healthy samples, the respective averages of the sensor responses are found to be equal to 240.34 (±37.10) and 219.63 (±41,62). For the 118 studied samples, the total mean value of the determined Euclidean norms is 230.51 (±40.46). The average value of the infected class is 20.71 units higher than that obtained for the healthy

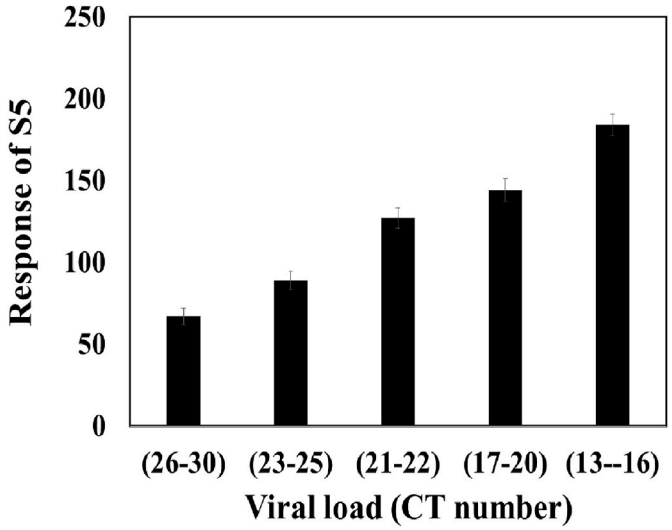

Fig. 5. The correlation between S5 response and the viral load obtained by rRT-PCR analysis. The experiment performed in the optimum conditions described in Fig. 2.

set. This difference with 95% confidence level is statistically significant (P_value < 0.005) based on the two independent sample *t*-test. Therefore, the Euclidean norms higher and lower than the total mean value are attributed to the patient and control samples, respectively.

3.6. The effect of volunteers' age on sensor responses

As mentioned earlier, the participants were selected from the male and female groups with the age range of 14–88 years. To investigate the effect of volunteers' age on the results of the experiment, the relationship between the parameter and the sensor responses was statistically evaluated.

The Pearson coefficient (0.023) and P-value (0.803) obtained confirm that no desirable and significant correlation is found between these two variables. Therefore, the discoloration of the sensing elements is solely due to metabolic changes caused by COVID-19 without being affected by the age of the studied population.

3.7. Determination of disease severity

Depending on the severity of the disease, the studied patients were divided into five categories: very mild, mild, moderate, severe and highly severe. The disease severity was specified based on the patient's medical information, including the symptoms of the disease and the rate of lung infection identified by chest imaging. The viral load values obtained by the rRT-PCR test (based on the cycle threshold (CT) value acquired for N gene) were also placed in the five ranges, consisting of (26–30), (23–25), (21–22), (17–20) and (13–16) for the very mild, mild, moderate, severe and highly severe groups, respectively. For each category, the response of the sensing elements was calculated. It is found that the color changes of receptor S5 (DWES + bromocresol purple) are correlated with increasing the disease severity (Fig. 5). The Euclidean norm values of sensor S5 are obtained to be 67, 89, 127, 144 and 184 for very mild, mild, moderate, severe and highly severe groups, respectively. The Pearson correlation coefficient for this relationship is 0.986 (P_value < 0.001). As a result, the proposed sensor can estimate the severity of the viral infection based on the response of sensor S5.

3.8. Reproducibility

Reproducibility is one of the effective parameters by which to evaluate the sensor performance in the achievement of a reliable response.

Table 3
Comparison between the performance of different analytical methods for discrimination of patients caused by COVID-19 and Healthy individuals through analysis of serum metabolites.

Analytical Method	Machine learning method	Sensitivity (%)	Specificity (%)	Accuracy (%)	Ref
LC-MS	PLS-DA	86.0–100.0	88.0–100.0	91.0–97.0	[49]
UPLC-MS/MS	RF	–	–	93.5	[50]
Raman spectroscopy	LDA	87.0	100.0	93.3	[51]
UPLC-MS	PLS-DA	97.0	97.0	97.0	[52]
GC/MS	PLS-DA	94	83	89	[53]
Gas sensor array	PLS-DA	94	80	89	[53]
Electronic tongue	PCA-DA	82.2	83.9	83.0	This work

LC-MS: Liquid Chromatography-tandem mass spectrometry, PLS-DA: Partial least squares-discriminant analysis, UPLC-MS/MS: Ultra performance liquid chromatography/tandem mass spectrometry, RF: Random forest, LDA: Linear discriminant analysis, GC/MS: Gas chromatography mass spectrometry.

To this end, a certain volume (20.0 μL) of a patient or control serum sample was initially injected to five individual paper sensors, followed by calculating the total sensor response. These response values are shown with bar graphs in Fig. S6 for each sample, along with the relative standard error percentage (RSD %). Accordingly, RSD values of the infected and healthy samples are reported to be 2.53% and 3.30%, respectively, indicating that the assay provides reproducible responses for the detection of the serum metabolites, and subsequently, for the diagnosis of COVID-19 diseases.

Table 3 represented the capability of the different analytical methods such as liquid Chromatography-tandem mass spectrometry, gas chromatography mass spectrometry, Raman spectroscopy and electronic nose including different gas sensors for detection of COVID-19 diseases by monitoring the metabolites of serum samples. The statistical results obtained by these assays were compared by those provided by the proposed electronic tongue. As expected, the accurate information was achieved using instrumental methods. In these studies, the statistical analysis were performed by a machine learning algorithm such as PLS-DA. However, the data of the proposed sensor can be comparable with those obtained by traditional device while the sensor responses were investigated by PCA-DA method. Also, the developed assay is more efficient in terms of price, design and fabrication process, on-site analysis, time of detection and user-friendliness. Therefore, this method can be consider as an appropriate device for rapid screening of disease through tracking the changes of the type and concentration of metabolites in the biological samples. Of course, the low specificity is a limiting factor for this method. This problem can be solved using the array with more number of sensing elements to detect the trace amount of chemical compounds with different structures or employing a powerful machine learning method to evaluate the sensor efficiency for discrimination of the two studied groups.

4. Conclusions

Based on the results of this study, it has been possible to monitor the serum metabolites of patients and control samples using a paper-based electronic tongue as a simple and user-friendly method for diagnosing COVID-19 diseases. The potential of the sensor to distinguish between the studied participants was visually confirmed by the evaluation of the colorimetric responses. The discrimination analysis also agreed with the comparison between the total responses of patient and control classes. Of course, the very mild severity of the disease in the patient or the healthy person provides unaccepted responses, limiting the accuracy of assay. The changes in the age of the participants had no effect on the sensor sensitivity in diagnosing the disease. The severity of the disease and the amount of viral load obtained from the PCR test could be estimated by determining the Euclidean norm of the sensing element S5. The statistical parameters of the classification analysis showed a good convergence between the results of the proposed sensor and those given by the standard clinical methods. The use of the portable paper-based sensor, cost-effective and available sensing elements, and small volumes of serum samples as well as the reproducible responses and on-site sample analysis, are the characteristics of the method presented in this study. So, colorimetric sensors and image analysis can be very useful for the screening in the disease especially for in the pandemic situation that we encounter with mass patients. However, for accurate detection, it should be used with gold standard assay.

Compliance with ethical standards

The research ethics committee of Baqiyatallah University of Medical Sciences has approved the project (Approval ID: IR. BMSU. REC.1399.508).

CRediT authorship contribution statement

Mohammad Mahdi Bordbar: Project administration, Methodology, Investigation, Formal analysis, Writing – original draft. **Hosein Samadinia:** Conceptualization, Methodology, Validation, Resources. **Azarmidokht Sheini:** Methodology, Validation. **Jasem Aboonajmi:** Methodology, Validation. **Pegah Hashemi:** Conceptualization, Methodology, Validation. **Hosein Khoshsafar:** Methodology, Validation. **Raheleh Halabian:** Methodology, Validation, Resources. **Akbar Khanmohammadi:** Methodology, Validation. **B. Fatemeh Nobakht M. Gh:** Conceptualization, Methodology, Validation. **Hashem Sharghi:** Conceptualization, Validation. **Mostafa Ghanei:** Conceptualization, Methodology, Validation, Resources. **Hasan Bagheri:** Conceptualization, Investigation, Supervision, Writing – review & editing.

Declaration of competing interest

The authors declare that they have no known competing financial interests or personal relationships that could have appeared to influence the work reported in this paper.

Data availability

Data will be made available on request.

Acknowledgments

The authors gratefully acknowledge the Research Council of Baqiyatallah University of Medical Sciences. Also, the authors would like to thank the Clinical Research Development Unit of Baqiyatallah Hospital, for all their support.

Appendix A. Supplementary data

Supplementary data to this article can be found online at https://doi.org/10.1016/j.aca.2022.340286.

References

[1] G. Giovannini, H. Haick, D. Garoli, Detecting COVID-19 from breath: a game changer for a big challenge, ACS Sens. 6 (2021) 1408–1417, https://doi.org/10.1021/acssensors.1c00312.

[2] B. Hu, H. Guo, P. Zhou, Z.L. Shi, Characteristics of SARS-CoV-2 and COVID-19, Nat. Rev. Microbiol. 19 (2021) 141–154, https://doi.org/10.1038/s41579-020-00459-7.

[3] WHO, Laboratory testing for 2019 novel coronavirus (2019-nCoV) in suspected human cases, WHO - Interim Guid. 2019 (2020) 1–7.

[4] L. Jansson, J. Hedman, Challenging the proposed causes of the PCR plateau phase, Biomol. Detect. Quantif. 17 (2019), https://doi.org/10.1016/j.bdq.2019.100082.

[5] M.M. Hellou, A. Górska, F. Mazzaferri, E. Cremonini, E. Gentilotti, P. De Nardo, I. Poran, M.M. Leeflang, E. Tacconelli, M. Paul, Nucleic acid amplification tests on respiratory samples for the diagnosis of coronavirus infections: a systematic review and meta-analysis, Clin. Microbiol. Infect. 27 (2021) 341–351, https://doi.org/10.1016/j.cmi.2020.11.002.

[6] N. Ravi, D.L. Cortade, E. Ng, S.X. Wang, Diagnostics for SARS-CoV-2 detection: a comprehensive review of the FDA-EUA COVID-19 testing landscape, Biosens. Bioelectron. 165 (2020), https://doi.org/10.1016/j.bios.2020.112454.

[7] A. Parihar, P. Ranjan, S.K. Sanghi, A.K. Srivastava, R. Khan, Point-of-Care biosensor-based diagnosis of COVID-19 holds promise to combat current and future pandemics, ACS Appl. Bio Mater. 3 (2020) 7326–7343, https://doi.org/10.1021/acsabm.0c01083. https://www.ncbi.nlm.nih.gov/pmc/articles/PMC7571308/?tool=EBI%0Ahttps://europepmc.org/article/PMC/PMC7571308.

[8] G. Rong, Y. Zheng, Y. Chen, Y. Zhang, P. Zhu, M. Sawan, COVID-19 diagnostic methods and detection techniques: a review, Ref. Modul. Biomed. Sci. (2021), https://doi.org/10.1016/b978-0-12-822548-6.00080-7.

[9] M.M. Bordbar, A. Sheini, P. Hashemi, A. Hajian, H. Bagheri, Disposable paper-based biosensors for the point-of-care detection of hazardous contaminations—a review, Biosensors 11 (2021), https://doi.org/10.3390/bios11090316.

[10] Janelle S. Ayres, A metabolic handbook for the COVID-19 pandemic, Nat. Metab. 2 (2020) 572–585.

[11] R. Baghel, K. Maan, T. Haritwal, P. Rana, Integration of epigenomics and metabolomics: from biomarkers discovery to personalized medicine, Epigenetics and Metabolomics (2021) 31–73, https://doi.org/10.1016/b978-0-323-85652-2.00002-6.

[12] G.A. Nagana Gowda, D. Raftery, Analysis of plasma, serum, and whole blood metabolites using 1H NMR spectroscopy, Methods Mol. Biol. 2037 (2019) 17–34, https://doi.org/10.1007/978-1-4939-9690-2_2.

[13] Z. Yu, G. Kastenmüller, Y. He, P. Belcredi, G. Möller, C. Prehn, J. Mendes, S. Wahl, W. Roemisch-Margl, U. Ceglarek, A. Polonikov, N. Dahmen, H. Prokisch, L. Xie, Y. Li, H.E. Wichmann, A. Peters, F. Kronenberg, K. Suhre, J. Adamski, T. Illig, R. Wang-Sattler, Differences between human plasma and serum metabolite profiles, PLoS One 6 (2011), https://doi.org/10.1371/journal.pone.0021230.

[14] H.O. Doğan, O. Şenol, S. Bolat, Ş.N. Yıldız, S.A. Büyüktuna, R. Sarıismailoğlu, K. Doğan, M. Hasbek, S.N. Hekim, Understanding the pathophysiological changes via untargeted metabolomics in COVID-19 patients, J. Med. Virol. 93 (2021) 2340–2349, https://doi.org/10.1002/jmv.26716.

[15] L. Lv, H. Jiang, Y. Chen, S. Gu, J. Xia, H. Zhang, Y. Lu, R. Yan, L. Li, The faecal metabolome in COVID-19 patients is altered and associated with clinical features and gut microbes, Anal. Chim. Acta 1152 (2021), https://doi.org/10.1016/j.aca.2021.338267.

[16] B. Shen, X. Yi, Y. Sun, X. Bi, J. Du, C. Zhang, S. Quan, F. Zhang, R. Sun, L. Qian, W. Ge, W. Liu, S. Liang, H. Chen, Y. Zhang, J. Li, J. Xu, Z. He, B. Chen, J. Wang, H. Yan, Y. Zheng, D. Wang, J. Zhu, Z. Kong, Z. Kang, X. Liang, X. Ding, G. Ruan, N. Xiang, X. Cai, H. Gao, L. Li, S. Li, Q. Xiao, T. Lu, Y. Zhu, H. Liu, H. Chen, T. Guo, Proteomic and metabolomic characterization of COVID-19 patient sera, Cell 182 (2020) 59–72, https://doi.org/10.1016/j.cell.2020.05.032, e15.

[17] C. Bruzzone, M. Bizkarguenaga, R. Gil-Redondo, T. Diercks, E. Arana, A. García de Vicuña, M. Seco, A. Bosch, A. Palazón, I. San Juan, A. Laín, J. Gil-Martínez, G. Bernardo-Seisdedos, D. Fernández-Ramos, F. Lopitz-Otsoa, N. Embade, S. Lu, J. M. Mato, O. Millet, SARS-CoV-2 infection dysregulates the metabolomic and lipidomic profiles of serum, iScience 23 (2020), https://doi.org/10.1016/j.isci.2020.101645.

[18] M.M. Bordbar, T.A. Nguyen, F. Arduini, H. Bagheri, A paper-based colorimetric sensor array for discrimination and simultaneous determination of organophosphate and carbamate pesticides in tap water, apple juice, and rice, Microchim. Acta 187 (2020), https://doi.org/10.1007/s00604-020-04596-x.

[19] P. Zhai, Y. Ding, X. Wu, J. Long, Y. Zhong, Y. Li, The epidemiology, diagnosis and treatment of COVID-19, Int. J. Antimicrob. Agents 55 (2020), https://doi.org/10.1016/j.ijantimicag.2020.105955.

[20] Q. Song, X. Sun, Z. Dai, Y. Gao, X. Gong, B. Zhou, J. Wu, W. Wen, Point-of-care testing detection methods for COVID-19, Lab Chip 21 (2021) 1634–1660, https://doi.org/10.1039/d0lc01156h.

[21] L. You, D. Zha, E.V. Anslyn, Recent advances in supramolecular analytical chemistry using optical sensing, Chem. Rev. 115 (2015) 7840–7892, https://doi.org/10.1021/cr5005524.

[22] M.M. Bordbar, J. Tashkhourian, B. Hemmateenejad, Structural elucidation and ultrasensitive analyses of volatile organic compounds by paper-based nano-optoelectronic noses, ACS Sens. 4 (2019) 1442–1451, https://doi.org/10.1021/acssensors.9b00680.

[23] M. Podrazka, E. Báczyńska, M. Kundys, P.S. Jeleń, E.W. Nery, Electronic tongue-A tool for all tastes? Biosensors 8 (2017) https://doi.org/10.3390/bios8010003.

[24] A. Sheini, A paper-based device for the colorimetric determination of ammonia and carbon dioxide using thiomalic acid and maltol functionalized silver nanoparticles: application to the enzymatic determination of urea in saliva and blood, Microchim. Acta 187 (2020), https://doi.org/10.1007/s00604-020-04553-8.

[25] M.M. Bordbar, T.A. Nguyen, A.Q. Tran, H. Bagheri, Optoelectronic nose based on an origami paper sensor for selective detection of pesticide aerosols, Sci. Rep. 10 (2020), https://doi.org/10.1038/s41598-020-74509-8.

[26] Y. Ma, Y. Li, K. Ma, Z. Wang, Optical colorimetric sensor arrays for chemical and biological analysis, Sci. China Chem. 61 (2018) 643–655, https://doi.org/10.1007/s11426-017-9224-3.

[27] Z. Li, J.R. Askim, K.S. Suslick, The optoelectronic nose: colorimetric and fluorometric sensor arrays, Chem. Rev. 119 (2019) 231–292, https://doi.org/10.1021/acs.chemrev.8b00226.

[28] M.M. Bordbar, H. Samadinia, A. Sheini, J. Aboonajmi, H. Sharghi, P. Hashemi, H. Khoshsafar, M. Ghanei, H. Bagheri, A colorimetric electronic tongue for point-of-care detection of COVID-19 using salivary metabolites, Talanta 246 (2022), 123537, https://doi.org/10.1016/j.talanta.2022.123537.

[29] M.M. Bordbar, H. Samadinia, A. Hajian, A. Sheini, E. Safaei, J. Aboonajmi, F. Arduini, H. Sharghi, P. Hashemi, H. Khoshsafar, M. Ghanei, H. Bagheri, Mask assistance to colorimetric sniffers for detection of COVID-19 diseases using exhaled breath metabolites, Sens. Actuators, B 369 (2022), 32379, https://doi.org/10.1016/j.snb.2022.132379.

[30] M.M. Bordbar, H. Samadinia, A. Sheini, J. Aboonajmi, M. Javid, H. Sharghi, M. Ghanei, H. Bagheri, Non-invasive detection of COVID-19 using a microfluidic-based colorimetric sensor array sensitive to urinary metabolites, Microchim. Acta 189 (2022) 316, https://doi.org/10.1007/s00604-022-05423-1.

[31] H. Sharghi, A.H. Nejad, Novel synthesis of meso-tetraarylporphyrins using CF3SO2Cl under aerobic oxidation, ChemInform 35 (2004), https://doi.org/10.1002/chin.200424113.

[32] D. Mansuy, Activation of alkanes : the biomimetic approach, Coord. Chem. Rev. 125 (1993) 129–141, https://doi.org/10.1016/0010-8545(93)85013-T.

[33] J. Bernadou, B. Meunier, A.S. Fabiano, A. Robert, Redox tautomerism" in high-valent metal-oxo-aquo complexes. Origin of the oxygen atom in epoxidation reactions catalyzed by water-soluble metalloporphyrins, J. Am. Chem. Soc. 116 (1994) 9375–9376, https://doi.org/10.1021/ja00099a083.

[34] J. Li, C. Hou, D. Huo, M. Yang, H.B. Fa, P. Yang, Development of a colorimetric sensor Array for the discrimination of aldehydes, Sens. Actuators, B 196 (2014) 10–17, https://doi.org/10.1016/j.snb.2014.01.054.

[35] R. Fu, C. Wang, J. Zhuang, W. Yang, Adsorption and desorption of DNA on bovine serum albumin modified gold nanoparticles, Colloids Surfaces A Physicochem. Eng. Asp. 444 (2014) 326–329, https://doi.org/10.1016/j.colsurfa.2013.12.081.

[36] A. Sheini, Colorimetric aggregation assay based on array of gold and silver nanoparticles for simultaneous analysis of aflatoxins, ochratoxin and zearalenone by using chemometric analysis and paper based analytical devices, Microchim. Acta 187 (2020), https://doi.org/10.1007/s00604-020-4147-5.

[37] M. Stevanović, I. Bračko, M. Milenković, N. Filipović, J. Nunić, M. Filipič, D. P. Uskoković, Multifunctional PLGA particles containing poly(l-glutamic acid)-capped silver nanoparticles and ascorbic acid with simultaneous antioxidative and prolonged antimicrobial activity, Acta Biomater. 10 (2014) 151–162, https://doi.org/10.1016/j.actbio.2013.08.030.

[38] S. Suvarna, U. Das, K.C. Sunil, S. Mishra, M. Sudarshan, K. Das Saha, S. Dey, A. Chakraborty, Y. Narayana, Synthesis of a novel glucose capped gold nanoparticle as a better theranostic candidate, PLoS One 12 (2017), https://doi.org/10.1371/journal.pone.0178202.

[39] A. Sheini, H. Khajehsharifi, M. Shahbazy, M. Kompany-Zareh, A chemosensor array for the colorimetric identification of some carboxylic acids in human urine samples, Sens. Actuators, B 242 (2017) 288–298, https://doi.org/10.1016/j.snb.2016.11.008.

[40] A. Sheini, M.D. Aseman, M.M. Bordbar, Origami paper analytical assay based on metal complex sensor for rapid determination of blood cyanide concentration in fire survivors, Sci. Rep. 11 (2021), https://doi.org/10.1038/s41598-021-83186-0.

[41] D.E. Booth, Chemometrics: data analysis for the laboratory and chemical plant, Technometrics 46 (2004), https://doi.org/10.1198/tech.2004.s738, 110–110.

[42] M.M. Bordbar, J. Tashkhourian, B. Hemmateenejad, Paper-based optical nose made with bimetallic nanoparticles for monitoring ignitable liquids in gasoline, ACS Appl. Mater. Interfaces 14 (2022) 8333–8342.

[43] S.H. Lim, C.J. Musto, E. Park, W. Zhong, K.S. Suslick, A colorimetric sensor array for detection and identification of sugars, Org. Lett. 10 (2008) 4405–4408, https://doi.org/10.1021/ol801459k.

[44] K. Suslick, K. Hulkower, A. Sen, M. Sroka, W. McNamara, Method and Apparatus for Detecting Ammonia from Exhaled Breath, US20050171449A1, 2005.

[45] Y. Wang, D. Huo, H. Wu, J. Li, Q. Zhang, B. Deng, J. Zhou, M. Yang, C. Hou, A visual sensor array based on an indicator displacement assay for the detection of carboxylic acids, Microchim. Acta 186 (2019), https://doi.org/10.1007/s00604-019-3601-8.

[46] Y. Mirzaei, A. Gholami, M.M. Bordbar, A distance-based paper sensor for rapid detection of blood lactate concentration using gold nanoparticles synthesized by Satureja hortensis, Sens. Actuators, B 345 (2021), https://doi.org/10.1016/j.snb.2021.130445.

[47] M.M. Bordbar, B. Hemmateenejad, J. Tashkhourian, S.F. Nami-Ana, An optoelectronic tongue based on an array of gold and silver nanoparticles for analysis of natural, synthetic and biological antioxidants, Microchim. Acta 185 (2018), https://doi.org/10.1007/s00604-018-3021-1.

[48] M.C. Janzen, J.B. Ponder, D.P. Bailey, C.K. Ingison, K.S. Suslick, Colorimetric sensor arrays for volatile organic compounds, Anal. Chem. 78 (2006) 3591–3600, https://doi.org/10.1021/ac052111s.

[49] A. de Fátima Cobre, M. Surek, D.P. Stremel, M.M. Fachi, H.H. Lobo Borba, F. S. Tonin, R. Pontarolo, Diagnosis and prognosis of COVID-19 employing analysis of

patients' plasma and serum via LC-MS and machine learning, Comput. Biol. Med. 146 (2022), 105659, https://doi.org/10.1016/j.compbiomed.2022.105659.

[50] B. Shen, X. Yi, Y. Sun, X. Bi, J. Du, C. Zhang, S. Quan, F. Zhang, R. Sun, L. Qian, W. Ge, W. Liu, S. Liang, H. Chen, Y. Zhang, J. Li, J. Xu, Z. He, B. Chen, J. Wang, H. Yan, Y. Zheng, D. Wang, J. Zhu, Z. Kong, Z. Kang, X. Liang, X. Ding, G. Ruan, N. Xiang, X. Cai, H. Gao, L. Li, S. Li, Q. Xiao, T. Lu, Y. Zhu, H. Liu, H. Chen, T. Guo, Proteomic and metabolomic characterization of COVID-19 patient sera, SSRN Electron. J. (2020), https://doi.org/10.2139/ssrn.3570565.

[51] A.C.C. Goulart, L. Silveira, H.C. Carvalho, C.B. Dorta, M.T.T. Pacheco, R. A. Zângaro, Diagnosing COVID-19 in human serum using Raman spectroscopy, Laser Med. Sci. 37 (2022) 2217–2226, https://doi.org/10.1007/s10103-021-03488-7.

[52] M. Spick, H.M. Lewis, C.F. Frampas, K. Longman, C. Costa, A. Stewart, D. Dunn-Walters, D.J. Skene, P. Barran, M.J. Wilde, G. Evetts, D. Greener, E. Sinclair, M. J. Bailey, An integrated analysis and comparison of serum, saliva and sebum for COVID-19 metabolomics, Res. Sq. Pre-Print (2022) 1–23.

[53] Y.K. Mougang, L. Di Zazzo, M. Minieri, R. Capuano, A. Catini, J.M. Legramante, R. Paolesse, S. Bernardini, C. Di Natale, Sensor array and gas chromatographic detection of the blood serum volatolomic signature of COVID-19, iScience 24 (2021), https://doi.org/10.1016/j.isci.2021.102851.